Science of the Total Environment 867 (2023) 161461

Contents lists available at ScienceDirect

Science of the Total Environment

journal homepage: www.elsevier.com/locate/scitotenv

Novel luminescence diagnosis of storm deposition across intertidal environments

Natascia Pannozzo [a,*], Rachel K. Smedley [a], Andrew J. Plater [a], Iacopo Carnacina [b], Nicoletta Leonardi [a]

[a] Department of Geography and Planning, School of Environmental Sciences, University of Liverpool, Chatham Street, Liverpool L69 7ZT, UK
[b] Department of Civil Engineering, School of Civil Engineering and Built Environment, Liverpool John Moores University, Byrom Street, Liverpool L3 3AF, UK

HIGHLIGHTS

- Storms do not always change the sediment composition of intertidal settings.
- Storm activity is currently undetectable if sediment composition does not change.
- Luminescence diagnosed differential modes of deposition across intertidal settings.
- This allowed storm detection in mudflats despite no change in sediment composition.

GRAPHICAL ABSTRACT

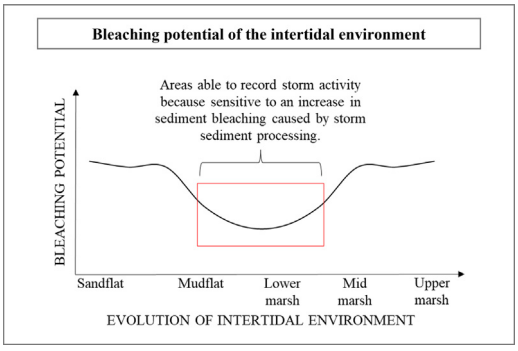

ARTICLE INFO

Editor: Ouyang Wei

Keywords:
Salt marshes
Mudflats
Intertidal environments
Storms
Luminescence

ABSTRACT

Salt marshes provide valuable nature-based, low-cost defences protecting against coastal flooding and erosion. Storm sedimentation can improve the resilience of salt marshes to accelerating rates of sea-level rise, which poses a threat to salt marsh survival worldwide. It is therefore important to be able to accurately detect the frequency of storm activity in longer-term sediment records to quantify how storms contribute to salt marsh resilience. Luminescence is able to infer how long mineral grains were exposed to sunlight prior to burial (e.g., the presence or absence of sediment processing). This study used sediment cores collected from the Ribble Estuary, North West England, to show that luminescence properties of sand-sized K-feldspar grains can diagnose the differential modes of deposition across intertidal settings (i.e., sandflat, mudflat and salt marsh) in longer-term sediment records by detecting the variability in sediment bleaching potential between settings (i.e., sediment exposure to sunlight), thus establishing a framework for the interpretation of luminescence properties of intertidal sediments. It then used modern sediment samples collected before and after a storm event to show how such properties can diagnose changes in sediment processing (i.e., bleaching potential) of mudflat sediments caused by storm activity, despite no changes in sediment composition being recorded by geochemical and particle size distribution analyses. This new luminescence approach can be applied to longer-term sediment records to reveal (and date) changes in the environment of deposition and/or depositional dynamics where there is no obvious stratigraphic evidence of such.

1. Introduction

Salt marshes provide valuable nature-based, longer-term, low-cost defences protecting against coastal flooding and erosion (e.g., Möller et al., 1999; Temmerman et al., 2013; Leonardi et al., 2018). Storm sedimentation can improve the resilience of salt marshes to accelerating rates of sea-level rise and

* Corresponding author.
E-mail address: sgnpanno@liverpool.ac.uk (N. Pannozzo).

http://dx.doi.org/10.1016/j.scitotenv.2023.161461
Received 4 October 2022; Received in revised form 1 January 2023; Accepted 4 January 2023
Available online 7 January 2023

decreasing sediment discharges of rivers (Mariotti and Fagherazzi, 2010; Schuerch et al., 2013; Yang et al., 2020; Pannozzo et al., 2021b), which pose a threat to salt marsh survival worldwide (e.g., Bakker et al., 1993; Environment Agency, 2011). Understanding the processes and longer-term frequency of storms that promote salt marsh resilience to sea-level rise is, therefore, a fundamental goal to ensure effective management of coastlines in the future (e.g., McCloskey and Liu, 2012; Walters and Kirwan, 2016; Bianchette et al., 2022). Salt marsh platforms do not record storm deposits uniformly, due to spatial constraints on sediment deposition caused by vegetation and topographic features characteristic of salt marsh surfaces. Tidal flats, conversely, represent a good archive for storm activity as there are fewer topographic and no vegetation constraints on sediment deposition. However, many storms process sediment locally rather than providing fresh input to the intertidal area (Grant et al., 1997; Wesselman et al., 2017; Brooks et al., 2017), causing no change in the tidal flat sediment composition (e.g., in particle size distribution or geochemistry); thus, existing techniques are not always able to detect storm activity in longer sediment records (Cundy et al., 1997). Solving this challenge requires a new approach to diagnosing storm activity in the geological record that does not rely upon a change in sediment composition.

The luminescence properties of mineral grains have been successfully used as a diagnostic tool of sediment dynamics (Gray et al., 2019), and deployed thus far as a sediment tracer to identify sediment sources and transport pathways in both coastal and fluvial settings (Sawakuchi et al., 2011, 2012, 2018; Ahmed et al., 2014; Haddadchi et al., 2016; Gray et al., 2017, 2018). Luminescence is based upon the principle that, when minerals (e.g., K-feldspars) are stimulated by light, heat or pressure, electrons that were stored in the crystal lattice are released, i.e. the luminescence signal is reset (or bleached) (see reviews by Smedley, 2018 and Murray et al., 2021). When subsequently buried, the minerals are exposed for a period of time to natural radiation (termed environmental dose-rate), which re-traps electrons within the crystal lattice and restores a luminescence signal (measured in the laboratory as equivalent dose, or D_e). In environments where sediments were exposed to sufficient duration and intensity of sunlight prior to burial, the luminescence signals of all of the grains are reset (i.e., well bleached) prior to burial. Where sunlight exposure prior to burial was insufficient, the luminescence signals reset partially (i.e., partially bleached). By determining D_e values from each sample, it is possible to determine how well bleached the mineral grains were before they were buried, and thus infer the nature of the bleaching environment (e.g., the presence or absence of sediment processing). The infra-red stimulated luminescence (IRSL) signals of K-feldspar have the potential to be used as a diagnostic tool of sediment dynamics due to the relative differences in bleaching rates of the multiple-elevated temperature (MET) post-infra-red infra-red stimulated luminescence (post-IR IRSL) signals measured at 50 °C (termed IR_{50}), 150 °C (termed $pIRIR_{150}$) and 225 °C (termed $pIRIR_{225}$) (e.g. Reimann et al., 2015; Chamberlain et al., 2017; Gray et al., 2017, 2018).

The aim of this study is to assess whether the luminescence properties of K-feldspars can be used to infer changes in sedimentation modes that have occurred in an intertidal setting. The Ribble Estuary, North West England, is used as a case study due to its ecological and economic value, and because storm surge deposits here are significant for the resilience of this salt marsh to sea-level rise (Lyons, 1997; Pannozzo et al., 2021a, 2021b). First, we test whether changes in sedimentation modes characteristic of the different intertidal settings (sandflat, mudflat and salt marsh) can be detected by the luminescence properties using a well-constrained, long-term, multi-proxy evolutionary analysis of the marsh platform (Pannozzo et al., 2022). Secondly, we use modern analogues collected before and after a storm event to assess whether luminescence can diagnose the greater opportunity for sunlight exposure (i.e., bleaching potential) caused by sediment processing from a storm event, which could be used to detect the storm activity preserved in sediment records that would otherwise go undetected using existing techniques.

2. Study site

The Ribble Estuary is a funnel-shaped, hypertidal estuary located in North West England (Fig. 1a), with an ordinary tidal range of 8.0 m at spring tide and 4.4 m at neap tide (UKHO, 2001). The marsh platform reaches 3 km at its widest and stands between ~ +3.2 m OD and ~ +4.7 m OD, while the intertidal flat reaches 2 km at its widest and stands between ~ +2 m OD and ~ +3 m OD. The extensive intertidal sand-silt flats and the salt marsh at the south of the estuary (Fig. 1b) resulted from the combination of infilling of sandy sediments from the bed of the Irish Sea and deposition of the silt and clay-size sediments coming from the River Ribble (van der Wal et al., 2002), with the majority of the sediment supply being marine in provenance (Wright et al., 1971; Pannozzo et al., 2022). The bed of the central Irish Sea is characterised by waves of mobile sediments that move up to 70 m per year (Van Landeghem et al., 2012), which can only be sustained because of the large sediment volumes deposited by ice retreating northwards up the Irish Sea during the last deglaciation (Van Landeghem and Chiverrell, 2020; Scourse et al., 2021). Tidal pumping, especially during high storm surges, is the main process introducing sediments into the estuary, increasing the sediment budget of the salt marsh with increasing storm surge intensity and duration (Lyons, 1997; Pannozzo et al., 2021a, 2021b). The moderate wave climate of the Ribble Estuary (Pye and Neal, 1994), that is insufficient to cause significant lateral erosion, is thought to have favoured the accretion of the marsh platform (van der Wal et al., 2002). Glacial Isostatic Adjustment models show a long-term decrease in the rate of relative sea-level rise in North West England for the past 2000 years (Tooley, 1974; Shennan et al., 2018). However, sea-level reconstructions and historical tidal gauge records show that, for the past ca. 240 years, the rate of sea-level rise has been increasing again (from ca. 0.39 mm yr^{-1} to ca. 2 mm yr^{-1}), thus causing an increase in the accommodation space (Plater et al., 1993; Woodworth et al., 1999; PSMSL, 2019). The salt marsh is covered predominantly by *Puccinellia maritima* and *Spartina townsendii*; the latest was planted in 1932 to aid the accretion of the marsh to favour land reclamation for agricultural purposes (van der Wal et al., 2002). Hesketh Out Marsh was reclaimed in 1980 and, between 2007 and 2017, a two-phase scheme was implemented to restore the intertidal habitat to enhance the protection of coastal infrastructures against flooding (Tovey et al., 2009).

3. Methods

3.1. Sampling strategy

To analyse the changes in bleaching potential in relation to salt marsh evolution and modes of deposition, Hesketh Out Marsh was cored using a percussion corer with a gouge 1 m long and 7.5 cm in diameter (Pannozzo et al., 2022). Two replicate cores 3.2 m long (HOM19-1 and HOM19-2) were extracted from the middle salt marsh next to one another at ~ +3.5 m OD (Fig. 1c). The middle salt marsh location provided a stratigraphic record from the formation of the sandflat through to a mature salt marsh, which was characterised by an accumulation rate spanning from 4.61 cm yr^{-1} in the sandflat to 0.83 cm yr^{-1} in the mature marsh. Core HOM19-1 was extracted in the sunlight and used for the analysis of the geochemical composition, organic content and particle size distribution. Core HOM19-2 was extracted into opaque sleeves to prevent sunlight contamination prior to luminescence analysis. Stratigraphic analysis showed that both cores contained similar stratigraphic patterns and were therefore comparable (Fig. 1d).

To assess whether luminescence properties could be used to diagnose the presence or absence (i.e. fair-weather conditions) of storm deposition across intertidal wetlands, modern analogues (Fig. 1c) were collected from the mudflat (~ +3 m OD) and lower salt marsh (~ +3.2 m OD) approximately one month before (HOM21-1 and HOM21-2) and after (HOM22-1 and HOM22-2) a storm event (Storm Barra as defined by the UK Met Office and Met Éireann). The storm hit the coast of North West England from 7th to 8th December 2021, during the transition from spring to neap tide, with wind gusts between 93 and 111 km h^{-1} in west-to-east direction (UK Met Office, 2021) that generated a storm surge of 0.5–0.9 m (BODC, 2021). The lower salt marsh and mudflat were chosen as the most suitable sampling locations based on the bleaching profile

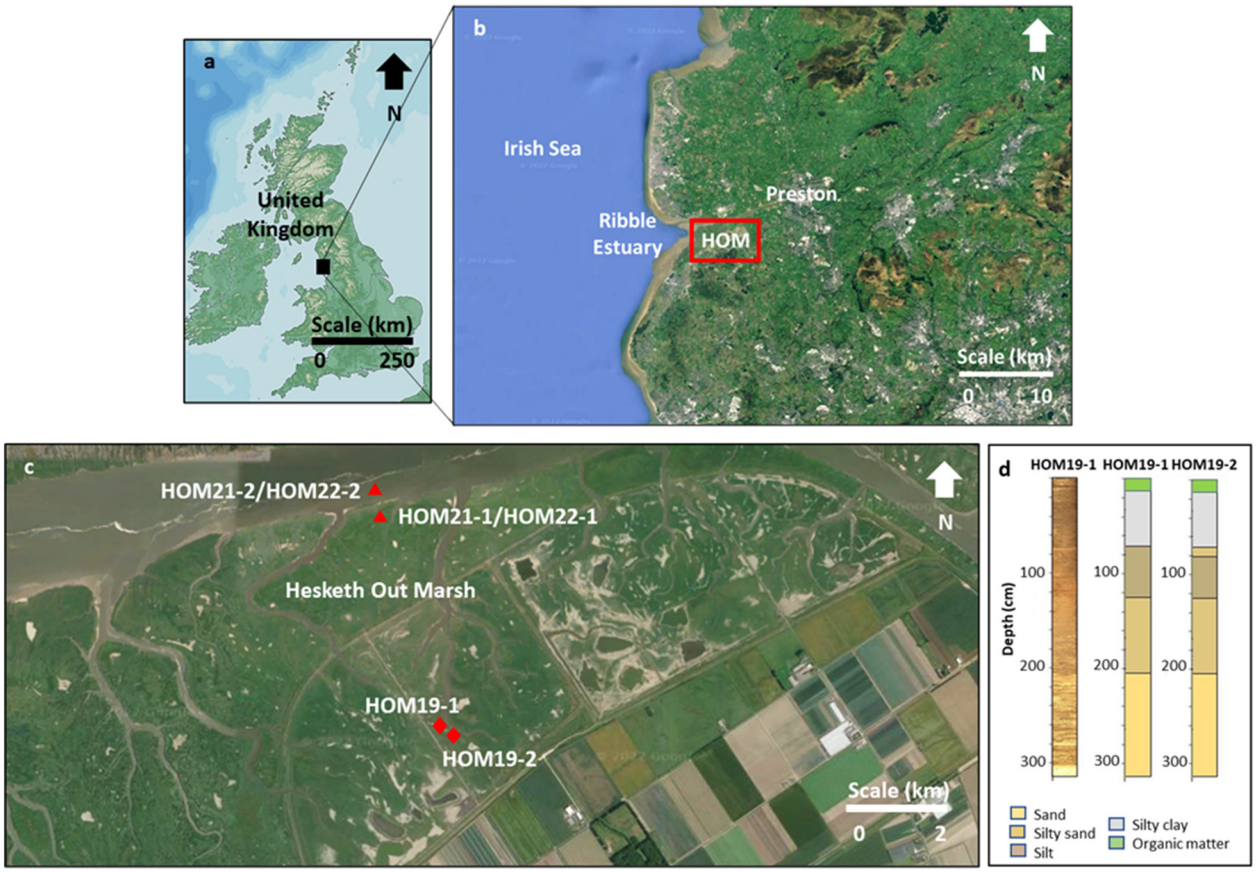

Fig. 1. Location of the Ribble Estuary (a); location of Hesketh Out Marsh (HOM) (b) (© Google Earth Pro); location of the cores HOM19-1 and HOM19-2 and the modern analogues collected before (HOM21-1 and HOM21-2) and after (HOM22-1 and HOM22-2) the storm event (c) (© Google Earth Pro); photographic analysis of the core HOM19-1 and stratigraphic analysis of the cores HOM19-1 and HOM19-2 (©Pannozzo et al., 2022) (d).

provided by the IRSL analysis performed on the core HOM19-2 (Fig. 2f). Each sample was combined from three superficial sub-samples (0.5–1.5 cm depths below the surface) collected using opaque tubes (10 cm in diameter) from 50 cm apart from each other to capture some of the spatial variability that could characterise this setting. Previous observations have shown that an ~1 m storm surge (comparable to the 0.5–0.9 m surge of Storm Barra) re-worked sediment down to ~15 cm below the mudflat surface in an unvegetated surface (de Vet et al., 2020); thus, the sampled sediment at 0.5–1.5 cm depths would avoid contamination from surface material that would have been exposed to sunlight since deposition while still preserving the signature of the storm activity.

All cores and samples are named according to the coring/sampling location (i.e., Hesketh Out Marsh) and year of the relative field campaign (i.e., 2019, 2021 and 2022).

3.2. Characterising different depositional environments

To characterise the geochemical composition and modes of deposition typical of each type of depositional environment (i.e., sandflat, mudflat or salt marsh), geochemical and particle size distribution (PSD) analyses were performed on core HOM19-1 by Pannozzo et al. (2022). Identical geochemical and PSD analyses were then performed on the modern analogues (both pre- and post- storms) in this study for comparison to core HOM19-1. A PSD model (Rahman and Plater, 2014) was used to infer whether sediment deposition was driven by accretion due to sea-level rise or infilling. Fine-skewed to near-symmetrical distributions characterised by well-sorted, sand-sized sediment are typical of traction load delivered by the fast tidal flow velocities (i.e., during the flood phase) and are attributable to infilling. Near-symmetrical distributions characterised by fine to very fine, poorly sorted silts are typical of the suspension load that settles during the turn of the tide (i.e., during the ebb phase) and is attributable to gradual accretion. Sandflats have low elevation and are flooded during high tide and so sediment deposition occurs through infilling as a result of the delivery of traction load during the flood phase. Salt marshes have high elevation; therefore, sediment deposition occurs as a result of the settling of suspension load during the turn of the tide. Mudflats are transitional environments characterised by a combination of the two processes. Principal component analysis (PCA) was performed using PAST3 (Hammer, 2019) and the correlation matrix to explore the geochemical compositions of the samples and to assess any association between the salt marsh core and the pre- and post- storm samples. The parameters selected for this PCA were: coarse mineral indicators (Si (mg/g), Zr (μg/g)), salt water (Na (mg/g),) and shell content indicators (Ca (mg/g), Sr (μg/g)), organic content indicators (LOI (%), S (mg/g), Br (μg/g)), silt/clay mineral indicators (K (mg/g), Al (mg/g), Ti (μg/g), Rb (μg/g), Nb (μg/g),), post-depositional diagenesis indicators (Fe (mg/g), Mn (μg/g)), pollutants (Mg (mg/g), P (mg/g), As (μg/g), Pb (μg/g), Zn (μg/g), Ni (μg/g), Cu (μg/g), V (μg/g), Cr (μg/g), Ga (μg/g), Ge (μg/g), Ba (μg/g), I (μg/g)) and the rare elements (Y (μg/g), La (μg/g), Ce (μg/g)) (Boyle, 2000; Plater et al., 2000).

To provide a robust evolutionary profile for the salt marsh platform alongside the depth profile of the PSDs, the PSD-derived median particle-size (D_{50}) were used alongside the chosen geochemical elements (Si/Al as sand indictor, Ca/K as shell indicator, Rb as fine mineral matter indicator and loss-on-ignition (LOI) as organic content indicator). Pannozzo et al. (2022) also derived a long-term accretion rate of the marsh platform from core HOM19-2 using luminescence dating of quartz. For further details on the conduction of these analyses see Pannozzo et al. (2022).

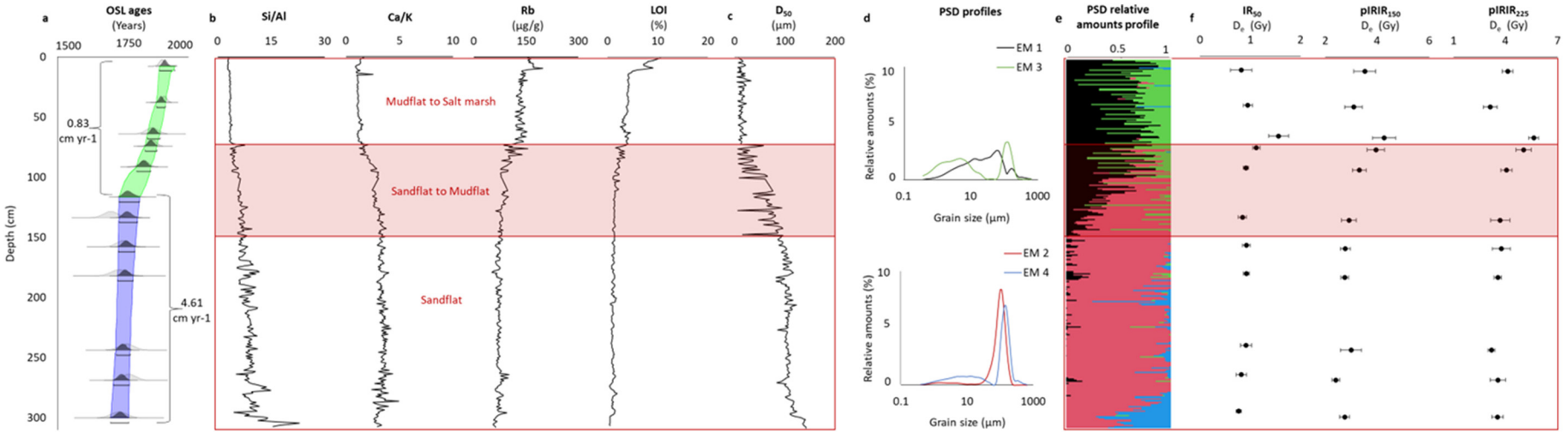

Fig. 2. Depth profile (core HOM19-2) of OSL ages with derived accretion rates (©Pannozzo et al., 2022) (a); depth profile (core HOM19-1) of geochemical proxies (Si/Al, Ca/K, Rb) and organic content (LOI) (©Pannozzo et al., 2022) (b); depth profile (core HOM19-1) of median particle-size (D_{50}) (©Pannozzo et al., 2022) (c); EMMA-derived PSD profiles (d) and depth profile (core HOM19-1) of the PSD relative amounts (e) (©Pannozzo et al., 2022); depth profile (core HOM19-2) of D_e (equivalent dose measured in Gy (J kg^{-1})) values calculated for IR_{50}, $pIRIR_{150}$ and $pIRIR_{225}$ signals (f).

3.3. Luminescence properties

Luminescence analyses were performed on sand-sized grains of K-feldspar extracted from the 12 core samples (HOM19-2) and the four modern analogue samples (HOM21-1/2 and HOM22-1/2). Each of the visible changes in core stratigraphy were sampled to capture the changing intertidal settings. At least 50 mm of the outer portion of each core sample was removed to prevent sunlight contamination. For the analysis of the modern analogues, three sub-samples per sample were extracted and combined for analysis, each from 0.5 to 1.5 cm depths below the surface to avoid contamination from surface material that would have been exposed to sunlight since deposition, but to still allow the signature of storm activity to be recorded. The degree of bleaching of the K-feldspar grains discussed here is intended as the cumulative product of pre-, during and post- depositional bleaching.

To isolate the coarse K-feldspar grains for equivalent dose (D_e) measurement, all samples were treated with a 10 % (v/v) dilution of 37 % HCl to dissolve carbonates and with a 10 % (v/v) dilution of H_2O_2 to remove organic content. Dry sieving was used to extract grains 90–150 μm in diameter for samples HOM19-2-2 and HOM19-2-4 and 90–125 μm for the rest of the samples. Density separation using sodium polytungstate was performed to isolate the K-feldspar fraction. However, no coarse-grained K-feldspar was recovered for sample HOM19-2-1 (top of the core) and so no analyses could be performed on this sample.

Grains were mounted as 2 mm-diameter multiple-grain aliquots on to 9.8 mm-diameter aluminium discs for analysis. The luminescence measurements were made using an automated Risø TL/OSL DA-15 reader equipped with a $^{90}Sr/^{90}Y$ source (Bøtter-Jensen et al., 2003). Infra-red (IR) light emitting diodes (LEDs) were used to stimulate the K-feldspar grains and the luminescence signals were detected in blue wavelengths using 2-mm thick Schott BG39 and Corning 7–59 filters. A single aliquot regeneration dose (SAR) protocol was used for determining D_e values, where the IRSL signal was recorded using a multiple-elevated post-IR IRSL protocol at 50 °C (termed the IR_{50}), 150 °C (termed the $pIRIR_{150}$) and 225 °C (termed the $pIRIR_{225}$) (Wallinga et al., 2000; Thomsen et al., 2008; Li and Li, 2011). Stimulation was for a total of 100 s, where the initial and background signals were summed for the first 3 s and final 40 s, respectively. Individual aliquots were screened for reliability of D_e determination based on the following screening criteria (considering the associated uncertainties): the test dose response was >3σ above the background; the test dose uncertainty was <20 %; the recycling ratio was ±20 %; and recuperation was <5 % of the response from the largest regenerative dose (7–8 Gy). Dose-recovery experiments performed on sample HOM19-2-6 using IR_{50} (ratio of 0.89 ± 0.00), $pIRIR_{150}$ (ratio of 0.91 ± 0.00) and $pIRIR_{225}$ (0.91 ± 0.03) signals showed that the measurement protocol was appropriate for luminescence analysis. Consequently, the central age model (CAM; Galbraith et al., 1999) was calculated from D_e distributions (Figs. S1, S2 and S3) determined for each sample to give an indication of the bleaching potential prior to burial. D_e is measured in Gy (J kg^{-1}).

4. Results

4.1. Luminescence properties of intertidal settings

The luminescence properties reflect the extent of sediment processing characterising each intertidal setting before sediment deposition. Overall, the multi-proxy analysis (Fig. 2; Pannozzo et al., 2022) shows that a sandflat environment dominates the lower part of the core up to 150 cm, while a transition from sandflat to mudflat occurs between 150 cm and 70 cm, followed by the mudflat gradually transitioning into a fully vegetated salt marsh. This is revealed by the Si/Al and Ca/K concentrations (indicators of shell and sand content, respectively, Fig. 2b) as well as the median particle-size (D_{50}, Fig. 2c), which are constant up to 100 cm, but decrease slightly up to 75 cm, before remaining constant to the top of the core. Also, the Rb concentrations (an indicator of fine mineral concentration) are constant up to 120 cm, but then decrease to the top of the core (Fig. 2b). Finally, loss on ignition (LOI) (an indicator of organic content concentration) is constant up to 100 cm, but then increases to the top of the core (Fig. 2b). Furthermore, the luminescence-derived accretion rates (from quartz; Pannozzo et al., 2022) show that up to 120 cm, the sequence experienced more rapid accretion (4.61 cm yr^{-1}) than the slower accretion (0.83 cm yr^{-1}) from 120 cm to the top of the core (Fig. 2a).

End-member analysis of the particle size distributions (PSDs) (Pannozzo et al., 2022) showed that 86 % of the variance present in core HOM19-1 could be explained by four PSD end-members (EM1, EM2, EM3 and EM4; Fig. 2d), each in different proportions within different samples from the core (Fig. 2e). These end-members represent the recurring modes detected in the PSDs: EM1 has a mixed near-symmetrical distribution dominated by clay to silt with a secondary very fine to fine sand mode; EM2 has a fine-skewed to near-symmetrical distribution dominantly very fine to fine sand; EM3 has a bimodal distribution with near-symmetrical clay to silt mode and near-symmetrical to fine skewed very fine to fine sand mode; and EM4 has a fine-skewed to near-symmetrical distribution of fine to coarse sand.

The PSD data empirically confirms that in the sandflat (300–150 cm depths) sediment deposition was mainly characterised by infilling of sand-sized particles through load traction (Fig. 2e). Here, the luminescence properties of all three luminescence signals (i.e., the D_e values) were constant (Fig. 2f), where the D_e distributions (representative of the degree of bleaching of the mineral grains) were symmetrical (i.e., well-bleached grains) (Fig. S1). As the sandflat progressed into a mudflat (150–70 cm depths), the sediment deposition was progressively dominated by more accretion through particle settling (Fig. 2e). Here, the luminescence properties increased (120–70 cm depths; Fig. 2f), where the D_e distributions were symmetrical for the IR_{50} signal but were near-symmetrical (i.e., well-bleached grains co-existing with poorly bleached grains) for the $pIRIR_{150}$ and $pIRIR_{225}$ signals (Fig. S1); thus, indicating a reduction in bleaching potential prior to burial of the sediment compared to the sandflat. Lastly, as the mudflat progressed into a salt marsh (70–0 cm depths), the sediment deposition was dominated by the settling of silt-sized particles (Fig. 2e). Here, the luminescence properties showed an increase first, followed by a non-linear decrease (Fig. 2f), suggesting an initial further decrease in the bleaching potential of the sediment followed by an increase once again. The D_e distributions were near-symmetrical (for the IR_{50} and $pIRIR_{150}$ signals) and symmetrical (for the $pIRIR_{225}$); however, the symmetrical nature of the $pIRIR_{225}$ may be due to the relatively smaller population for this signal.

4.2. Luminescence properties of pre- and post-storm deposits

Fig. 3 shows the first two components of the PCA performed on the geochemical properties of the salt marsh and mudflat samples. Component 1 and component 2 summarise 76.9 % of the variance in the data, respectively 66.4 % and 10.5 %. Based on the correlation, the PCA analysis shows that the pre- and post-storm samples form a single cluster (i.e., the geochemical composition of the pre-storm sediments is statistically indistinguishable from the composition of the post-storm sediment), and that the composition of the modern samples differs from that of the core largely due to the absence of historical heavy metal pollution post-depositional diagenesis.

Overall, Fig. 4 shows that the luminescence properties of the sediments collected post-storm were different to those collected pre-storm, likely reflecting the greater extent of sediment processing that occurs during a storm and agrees with the trends observed in the down-core profile.

For the salt marsh sample, there is a small change in the shape of the PSD profile after the storm surge (Fig. 4a). Before the storm, the salt marsh sample exhibits a near-symmetrical distribution characterised by fine to very fine silts but with a wider range than the post-storm sample, which exhibits fine-skewed to near-symmetrical distribution. For all three luminescence signals, the D_e values of the salt marsh sample collected before the storm and after the storm are all statistically indistinguishable, i.e. mean D_e values and relative uncertainties of the two samples overlap

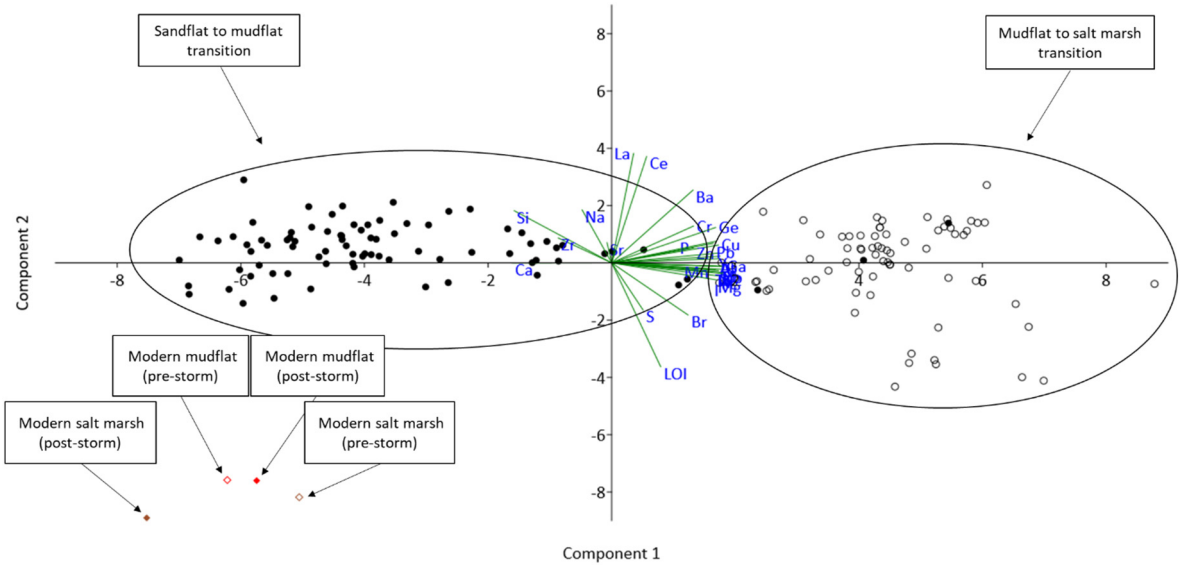

Fig. 3. PCA performed on the salt marsh and mudflat modern analogues collected before (HOM21-1/2) and after (HOM22-1/2) the storm and the core (HOM19-1) intervals (©Pannozzo et al., 2022) showing sandflat-to-mudflat (150–70 cm depths) and mudflat-to-salt marsh (70–0 cm) transitions. Component 1 and component 2 summarise 76.9 % of the variance in the data, respectively 66.4 % and 10.5 %. The figure shows the parameters used by each component to separate the samples. The modern mudflat and salt marsh deposits differ from their paleo counterparts due to lower concentrations of heavy metals.

for all signals. The density of the D_e distributions for the pre- and post-storm salt marsh samples do not differ significantly as they are predominantly symmetrical to near-symmetrical in both cases (Fig. S2).

For the mudflat sample, both the pre- and post-storm PSD profiles exhibit very similar fine-skewed to near-symmetrical distributions characterised by coarse to fine silts, with the post-storm PSD profile only showing slightly higher kurtosis (Fig. 4a). Interestingly, the post-storm PSD profile for the mudflat was very similar to the salt marsh, demonstrating that the mudflat and salt marsh experienced the same depositional dynamics from the storm. There was little difference in the IR_{50} signal before and after the storm on the mudflat as the D_e value of the post-storm sample was slightly higher than the pre-storm sample but overlapped within uncertainties. In contrast, the D_e values of the post-storm samples were lower than the D_e values of the pre-storm samples for both the $pIRIR_{150}$ and $pIRIR_{225}$ signals. This suggests that sediments in a mudflat setting experience more bleaching from sediment processing during a storm surge than during fair weather conditions, which is not recorded on the lower salt marsh. The mudflat samples had symmetrical to near-symmetrical D_e distributions in both cases, however, the post-storm distributions become wider for all three signals, suggesting that a small proportion of grains with larger D_e distribution was incorporated into the sediment post-storm, in addition to the overall reduction in CAM D_e value.

5. Discussion

5.1. Sediment processing in intertidal settings

Luminescence properties were used to diagnose the changes in sediment processing characteristic of different intertidal settings (sandflat, mudflat, salt marsh) based on the bleaching potential of the feldspar grains present in intertidal sediments (Reimann et al., 2015). In the sandflat environment (300–120 cm; Fig. 2b, c) (Plater et al., 2007), the luminescence properties (i.e., the D_e values calculated for the IR_{50}, $pIRIR_{150}$ and $pIRIR_{225}$ signals) were constant (Fig. 2f) and the average accretion rate was higher than the upper sequence (4.61 cm yr^{-1}; Fig. 2a). With the transition from the sandflat into a mudflat (120–70 cm depths; Fig. 2b, c) (Plater et al., 2007), the average accretion rate decreased (0.83 cm yr^{-1}; Fig. 2a) and the luminescence properties showed

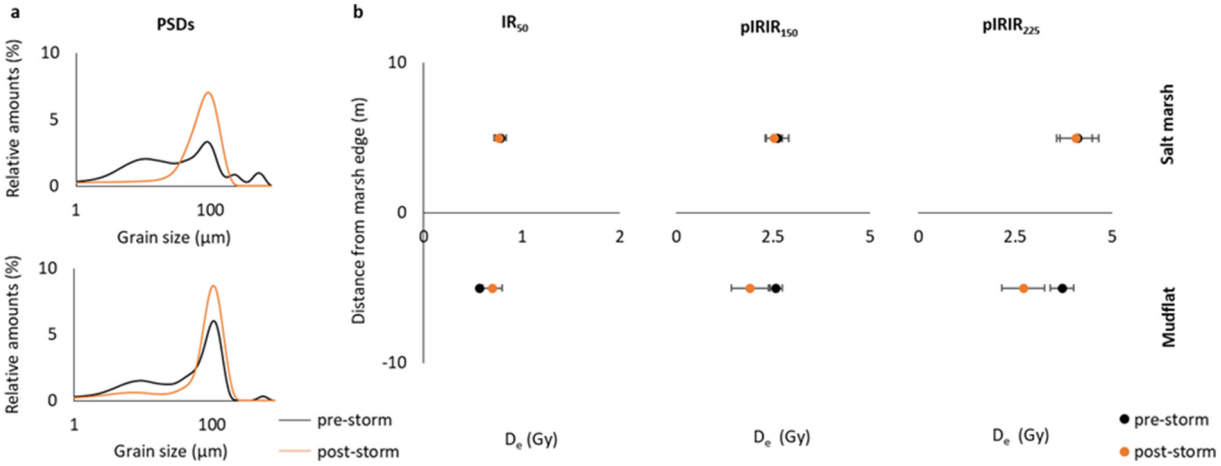

Fig. 4. EMMA-derived PSD profiles (a) and D_e (equivalent dose measured in Gy (J kg^{-1})) values relative to the IR_{50}, $pIRIR_{150}$ and $pIRIR_{225}$ signals (b) for the salt marsh and mudflat modern analogues collected before (HOM21-1/2) and after (HOM22-1/2) the storm.

progressive increases in D_e values (Fig. 2f). Between 70 cm and the top of the core, where the well-established mudflat transitions into the fully-vegetated salt marsh (Fig. 2b, c) (Plater et al., 2007), the average accretion rate was maintained (0.83 cm yr^{-1}; Fig. 2a) and the luminescence properties showed an initial further increase followed by progressive decreases in D_e values similar to the sandflat (Fig. 2f).

The luminescence properties showed that the bleaching potential was high in the sandflat, where the extent of sediment processing is large. It then decreased with the formation of a mudflat and transition into a vegetated salt marsh environment but increased again with the transition into a mature marsh, where sediments are directly exposed to sunlight for long periods of time. These changes in the bleaching potential of the sediments were also reflected in the D_e distributions (Fig. S1), which were representative of the degree of bleaching of the mineral grains. The D_e distributions for all three signals for the sandflat were symmetrical, indicating well-bleached grains. The D_e distribution for the IR_{50} signal for the mudflat was broadly symmetrical but bimodal, and near-symmetrical for the $pIRIR_{150}$ and $pIRIR_{225}$ signals, suggesting poorer bleaching of the grains. Finally, in the salt marsh, the D_e distributions were near-symmetrical to symmetrical again for all three signals, indicating that the grains were again better bleached (Wallinga, 2002a).

PSD analysis of the core (Fig. 2d, e) shows that from 300 to 150 cm, the two dominant modes (EM4 and EM2) exhibit fine-skewed to near-symmetrical distributions characterised by well-sorted, sand-sized sediment. Sandflats have an elevation low enough to allow the platform to be permanently flooded and experience the fastest tidal currents (Reed, 1990); hence, sediment deposition occurs through infilling resulting from the delivery of traction load by the fast tidal flow velocities during the flood phase (Rahman and Plater, 2014). When the sandflats evolve into mudflats, the elevation of the platform increases, and they start experiencing slower tidal currents (Reed, 1990). Therefore, deposition gradually progresses from being dominated by infilling of sand-sized sediment to being dominated by silt-sized particles that are transported by the fast tidal flow velocities during the flood phase and deposited through settling during the turn of the tide (Rahman and Plater, 2014). This is reflected in the down-core PSDs profile, which shows that at 150 cm EM4 (fine-skewed to near-symmetrical distribution of fine to coarse sand) is replaced by EM1 (mixed near-symmetrical distribution dominated by clay to silt with a secondary very fine to fine sand mode), and the mode of deposition becomes dictated by EM2 (fine-skewed to near-symmetrical distribution dominantly very fine to fine sand) and EM1, with EM1 becoming more influential towards the top of the section.

Salt marsh platforms have higher elevation with respect to mudflats where the frequency and duration of inundation depend on the level of maturity of the salt marsh platform and distance from the marsh edge (van Proosdij et al., 2006), with mature marshes being inundated only a few times a year due to very high spring tides or storm surges (Roberts and Plater, 2005). Hence, sediment deposition occurs mainly from the settling of the suspension load during the turn of the tide (Rahman and Plater, 2014). This is reflected in the down-core PSDs profile, which shows the mode of deposition being dictated by EM3 (bimodal distribution with near-symmetrical clay to silt mode and near-symmetrical to fine skewed very fine to fine sand mode) and EM1 (mixed near-symmetrical distribution dominated by clay to silt with a secondary very fine to fine sand mode), both characterised by a near-symmetrical clay to silt mode, representative of the sediment settling, and near-symmetrical to fine skewed, very fine to fine sand mode, representative of the infilling events.

The bleaching potential of K-feldspar grains depends on the duration and intensity of sunlight exposure (Godfrey-Smith et al., 1988). In turbulent water columns, this can be affected by the degree of sediment processing in the water column during deposition (Wallinga, 2002b). This suggests that the different elevations and modes of deposition characteristic of each type of intertidal environment (sandflat, mudflat and salt marsh) are responsible for the different degrees of bleaching of the K-feldspar grains. Fig. 5 shows a schematic of how the bleaching potential of intertidal sediments varies with the evolution of the intertidal substrate in proportion to the hydroperiod, the wave and tidal current induced shear stress, and the duration of sunlight exposure during the period of sub-aerial exposure. The duration and frequency of flooding on the intertidal platform (i.e., hydroperiod) and the sheer stress magnitude are higher for a sandflat with low elevation, and they decrease with the increase in elevation of the platform (Roberts and Plater, 2005; Zhang et al., 2019), up to a point when a mature marsh forms, which is inundated only a few times a year by very high spring tides or storm surges (Pethick, 1981). Direct exposure to sunlight during the period of sub-aerial exposure conversely increases with an increase in elevation of the intertidal platform as it reaches its maximum when the hydroperiod and shear stress are at their minimum.

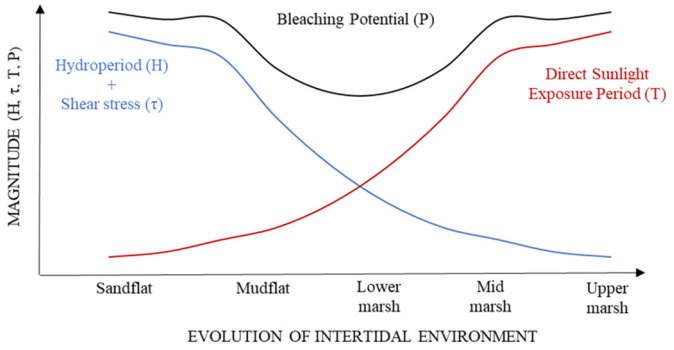

Fig. 5. Schematic of variation in bleaching potential of intertidal sediments (P) in relation to the evolution of the intertidal environment, hydroperiod (H), wave and tidal current induced shear stress (τ), and period of direct exposure to sunlight after deposition (T).

In the sandflat, where the magnitude of the hydroperiod and the shear stress is high (Zhang et al., 2019), the traction load deposited on the platform can be re-entrained and resuspended within the water column for multiple tidal cycles before being buried by new sediment. This continuous re-entrainment allows sediments to be exposed to sunlight for a period of time long enough for the luminescence signal to reset to zero, and it is recycled several times on a series of tides (Wallinga, 2002b). When the sandflat progresses into a mudflat and the platform elevation increases, the hydroperiod and shear stress decrease (Zhang et al., 2019), which causes less re-entrainment and resuspension of the traction load and reduces the recycling of sediment on each tide. Moreover, as the mudflat increases in elevation, the suspension load that settles during the turn of the tide progressively replaces the traction load transported by the flood tide. This causes less opportunity for the sediment to be re-entrained and re-suspended by the fast tidal currents before being buried by new sediments, leading to less sunlight exposure, and therefore less potential for the luminescence signal to have been well bleached prior to burial (Wallinga, 2002b). Turbidity caused by mud in suspension can further promote partial bleaching of the luminescence signals by attenuating the blue wavelengths of the daylight spectrum, inhibiting the bleaching of the grains (Berger, 1990).

As the mudflat progresses into a lower salt marsh, the influence of the hydrodynamic on the resetting of the luminescence signal becomes minimal, as the presence of vegetation attenuates the resuspension caused by waves and currents (Neumeier and Ciavola, 2004; Mudd et al., 2010; Yang et al., 2012), and the sediments are mainly deposited during the turn of the tide, thus causing a further decrease in bleaching potential. Finally, on the mature salt marsh, where there is no inundation and sediments are continuously exposed to sunlight, grains reach their maximum bleaching potential (Godfrey-Smith et al., 1988). Overall, the long-term analysis suggests that luminescence properties can detect the different sedimentation modes balanced across the bleaching potential and sediment processing potential typical of each intertidal setting.

5.2. Sediment processing during storm events

The luminescence properties of the down-core profile show that the mudflat and lower salt marsh are the environments with the lowest

bleaching potential (Fig. 2f). Therefore, since storms are responsible for longer inundation and higher potential sediment resuspension compared to ordinary conditions (Pannozzo et al., 2021a, 2021b), mudflat and lower salt marsh (where topography and vegetation allow deposition) sediments are expected to be the most likely to show an increase in bleaching during stormy conditions (Brill et al., 2018). Hence, they have been selected in this study as locations for the sampling of the modern analogues (Fig. 1c). Both mudflat and salt marsh sediments show no significant difference in the geochemical composition (Fig. 3) and a slight variability in the gross depositional energy (Fig. 4a) between the pre- and post- storm samples, providing a weak inference of the storm event from the lower salt marsh but none from the mudflat.

The storm occurred during spring tide and caused a surge of 0.5–0.9 m (BODC, 2021). During spring high tide, the water depth above the lower marsh platform at Hesketh Out Marsh can reach up to 3 m in fair-weather conditions and a surge of 0.5 m can cause an increase in the depth of the water level of 0.5 m (Pannozzo et al., 2021a). This suggests that the storm-enhanced inundation of the salt marsh caused an increase in the extreme water level by at least 0.5 m, potentially reaching up to at least 3.5 m during high tide. Furthermore, the surge peak occurred towards the lower end of the tide, coinciding with the rising flood tide, thus promoting the most optimal conditions for sediment re-entraining and recycling (Pannozzo et al., 2021b). Despite that, the luminescence properties of the salt marsh sample collected before and after the storm were indistinguishable (Fig. 4b; Fig. S2), suggesting that the storm surge did not cause any significant change in the bleaching potential of the lower marsh sediment. The long-term multi-proxy analyses showed that the lower salt marsh was suitable for detecting a possible increase in the resetting of the luminescence signal caused by a storm surge (Brill et al., 2018), due to its low natural bleaching potential. However, it must be considered that vegetation causes a reduction in the turbulent kinetic energy of the water flow, causing a considerable reduction in shear stresses produced by the combined action of waves and currents, therefore reducing the potential for sediment resuspension (Neumeier and Ciavola, 2004; Mudd et al., 2010; Yang et al., 2012; Temmerman et al., 2022). This might have prevented sediment re-entrainment and recycling during the inundation of the lower marsh and inhibited the bleaching of the grains.

For the mudflat, there was a difference between the sediments collected before and after the storm surge for the higher temperature signals ($pIRIR_{150}$ and $pIRIR_{225}$ signals), but not for the IR_{50} signal (Fig. 4b). The IR_{50} signal bleaching rate is on the order of seconds to minutes (Godfrey-Smith et al., 1988), while the $pIRIR_{150}$ and $pIRIR_{225}$ signals can take up to hours to completely reset according to laboratory measurements (e.g., Smedley et al., 2015; Colarossi et al., 2015). This suggests that the IR_{50} signal is likely to reset completely even if sediments do not spend a long period in suspension within the water column (Brill et al., 2018), whereas the $pIRIR_{150}$ and $pIRIR_{225}$ signals are more likely to show partial resetting if sediments are not exposed to sunlight for a sufficient duration of time (Reimann et al., 2015). As such, the IR_{50} signal is likely to reset in both ordinary and stormy conditions, while the $pIRIR_{150}$ and $pIRIR_{225}$ signals are likely to bleach faster in stormy conditions when sediments are resuspended in the water column for longer or transported for longer distances. The $pIRIR_{150}$ and $pIRIR_{225}$ signals are therefore likely to be more reliable in diagnosing changes in the bleaching potential of the grains with respect to the IR_{50} signal. The change in bleaching potential characterising the mudflat after the storm event is also evident in the D_e distributions of single aliquots (Fig. S2), which shows a widening of the distributions for all three signals. The overall reduction in D_e values suggests that autochthonous sediments could have bleached better in stormy conditions because the longer inundation maintained them in re-suspension longer than in fair-weather conditions, or that allochthonous, well-bleached sediments were transported onto the mudflat platform while they were maintained in suspension within the water column (Brill et al., 2018). The small proportion of grains with larger D_e distributions could have come from sediments unlikely to have been exposed to sunlight where the enhanced mud re-suspension caused by the storm is likely to have enhanced turbidity, potentially preventing the exposure to sunlight (i.e. bleaching) of those grains (Berger, 1990). Regardless of the provenance and/or composition of the well-bleached sediment (i.e., autochthonous, or allochthonous), the D_e distributions are able to detect the increase in bleaching rate caused by the storm.

Overall, the modern analogues have shown that the samples collected after the storm event on the mudflat were characterised by no significant change in sediment composition, but the post-storm sediments exhibited higher bleaching potential than the pre-storm samples, which suggests a greater extent of sediment processing; thus, luminescence could be used to diagnose the storm deposition on the mudflat where the sediment composition could not. In contrast, there was no difference in the bleaching potential pre- and post-storm on the lower salt marsh.

5.3. Implications

There is evidence that increasing rates of sea-level rise can threaten salt marsh survival (FitzGerald et al., 2008; Kirwan et al., 2010; Ganju et al., 2017; Fagherazzi et al., 2020), while storm-sedimentation can support salt marsh resilience to sea-level rise (Mariotti and Fagherazzi, 2010; Schuerch et al., 2013; Pannozzo et al., 2021b). To provide effective management of these natural coastal defences and ecosystems, it is essential to quantify the contribution of sea level and storm activity to long-term marsh accretion and survival (Walters and Kirwan, 2016) and to derive long-term records of storm frequency that can contextualise the changes observed by recent climate change (McCloskey and Liu, 2012; Bianchette et al., 2022). Traditional techniques used to detect sedimentary records of storm activity (i.e., geochemical and particle size analysis) in mudflat settings cannot detect storm-driven changes in hydrodynamics when no change in sediment composition has occurred, as recorded during Storm Barra. Therefore, longer-term sediment grain size and geochemical composition records cannot readily provide accurate records of the frequency of storm activity. The new luminescence approach shown here can reveal (and date) changes in the extent of sediment processing (e.g., storm activity) where there is no obvious stratigraphic evidence of such that could be revealed by the existing techniques (e.g., the sediment composition). Applying this luminescence approach, and associated dating, to established sedimentary archives of coastal change in estuary and deltaic depositional contexts (e.g., Yangtze Estuary, Rhine-Meuse lowlands) would therefore more accurately constrain the contribution and significance of storms in moderating coastal change over the long term, e.g. during periods of sea-level rise throughout the last interglacial and the Holocene. This has far-reaching consequences for projecting future coastal response to sea-level rise and changes in storm activity by providing an improved assessment of the resilience of populated coastal lowlands to climate change.

6. Conclusions

To conclude, this study has shown how luminescence properties can be used to diagnose the differential modes of deposition across intertidal settings, and therefore the presence of storm activity in the longer-term sediment records where no changes in sediment composition occurred. The luminescence signals of K-feldspars measured at different temperatures (50, 150 and 225 °C) reset at inherently different rates and so were used to assess the extent of sediment processing (i.e., the bleaching potential) in an environment during deposition. Analysis of a long-term, multi-proxy evolutionary model of the marsh platform showed that the luminescence properties of mineral grains can be used to diagnose changes in sedimentation modes characteristic of the different intertidal settings (sandflat, mudflat and salt marsh) by detecting the variability in sediment bleaching potential between settings (i.e., sediment exposure to sunlight), thus establishing a framework for the interpretation of luminescence properties of intertidal sediments. Modern analogue samples showed that post-storm sediments exhibited higher bleaching potential detectable by the $pIRIR_{150}$ and $pIRIR_{225}$ signals (i.e., more sediment processing) on the mudflat prior to burial in comparison to the pre-storm samples, despite no significant

change in sediment composition being recorded by the geochemical and particle size distribution analyses. This new luminescence approach is more sensitive than existing techniques at detecting the intertidal response to sea level and/or storms, and so can accurately identify periods of change that were previously undetectable in apparently monotonous minerogenic sequences. This offers the potential to revise established sedimentary archives of coastal change and determine with more accuracy the significance of storms in controlling coastal change over the longer-term during climate warming, e.g. the Holocene and the last interglacial.

CRediT authorship contribution statement

Natascia Pannozzo: Conceptualization, Data curation, Formal analysis, Investigation, Methodology, Project administration, Writing – original draft. **Rachel K. Smedley:** Conceptualization, Funding acquisition, Investigation, Methodology, Resources, Supervision, Writing – review & editing. **Andrew J. Plater:** Investigation, Resources, Writing – review & editing. **Iacopo Carnacina:** Investigation, Resources, Supervision, Writing – review & editing. **Nicoletta Leonardi:** Funding acquisition, Investigation, Resources, Supervision, Writing – review & editing.

Data availability

Data related to this article can be found in the following repository: https://doi.org/10.5281/zenodo.7378526.

Declaration of competing interest

The authors declare that they have no known competing financial interests or personal relationships that could have appeared to influence the work reported in this paper.

Acknowledgements

We acknowledge support from the School of Environmental Sciences, University of Liverpool, which is funding the PhD project of the first author, the EPSRC support to Prof. Nicoletta Leonardi (EP/V056042/1) and the RGS-IBG for funding part of the field campaign (project title: Building coastal resilience one sediment grain at the time: field measurements and community engagement on nature-based solutions for coastal protection, PI Prof. Nicoletta Leonardi). We also acknowledge the support of the RSPB for allowing the fieldwork campaign in the Ribble Estuary and the Geography and Luminescence laboratories and their technicians and students (Jennifer Bradley, Luke Glascott, Mike O'Connor, Richard Clark, Grace Skirrow and Molly Spater) for their support with equipment, fieldwork and laboratory analyses. The content from Pannozzo et al. (2022) was reproduced under the CC BY 4.0 licence. We ultimately thank two anonymous reviewers for their constructive feedback on the manuscript.

Appendix A. Supplementary data

Supplementary data to this article can be found online at https://doi.org/10.1016/j.scitotenv.2023.161461.

References

Ahmed, M.T., Sato, S., Tajima, Y., 2014. Quantitative estimation of longshore sediment transport based on thermoluminescence: two case studies around Tenryu and Nile River Mouths. J. Coast. Res. 30 (3), 537–547. https://doi.org/10.2112/JCOASTRES-D-13-00050.1.

Bakker, J.P., de Leeuw, J., Dijkema, K.S., Leendertse, P.C., Prins, H.H., Rozema, J., 1993. Salt marshes along the coast of the Netherlands. Hydrobiologia 265, 73. https://doi.org/10.1007/BF00007263.

Berger, G.W., 1990. Effectiveness of natural zeroing in of the thermoluminescence in sediments. J. Geophys. Res. 95, 12375–12397. https://doi.org/10.1029/JB095iB08p12375.

Bianchette, T.A., Liu, K., McCloskey, T.A., 2022. A 4000-year paleoenvironmental reconstruction and extreme event record from Laguna Nuxco, Guerrero, Mexico. Palaeogeogr. Palaeoclimatol. Palaeoecol. 594, 110933. https://doi.org/10.1016/j.palaeo.2022.110933.

BODC, 2021. British Oceanographic Data Centre. National Oceanography Centre, Liverpool https://www.bodc.ac.uk.

Bøtter-Jensen, L., Andersen, C.E., Duller, G.A.T., Murray, A.S., 2003. Developments in radiation, stimulation and observation facilities in luminescence measurements. Radiat. Meas. 37, 535–541. https://doi.org/10.1016/S1350-4487(03)00020-9.

Boyle, J.F., 2000. Rapid elemental analysis of sediment samples by isotope source XRF. J. Paleolimnol. 23, 213–221. https://doi.org/10.1023/A:1008053503694.

Brill, D., Reimann, T., Wallinga, J., May, S.M., Engel, M., Riedesel, S., Brückner, H., 2018. Testing the accuracy of feldspar single grains to date late Holocene cyclone and tsunami deposits. Quat. Geochronol. 48, 91–103. https://doi.org/10.1016/j.quageo.2018.09.001.

Brooks, S.M., Spencer, T., Christie, E.K., 2017. Storm impacts and shoreline recovery: mechanisms and controls in the southern North Sea. Geomorphology 283, 48–70. https://doi.org/10.1016/j.geomorph.2017.01.007.

Chamberlain, E.L., Wallinga, J., Reimann, T., Goodbred Jr., S.L., Steckler, M.S., Shen, Z., Sincavage, R., 2017. Luminescence dating of delta sediments: novel approaches explored for the Ganges-Brahmaputra-Meghna Delta. Quat. Geochronol. 41, 97–111. https://doi.org/10.1016/j.quageo.2017.06.006.

Colarossi, D., Duller, G.A.T., Roberts, H.M., Tooth, S., Lyons, R., 2015. Comparison of paired quartz OSL and feldspar post-IR IRSL dose distributions in poorly bleached fluvial sediments from South Africa. Quat. Geochronol. 30, 233e238. https://doi.org/10.1016/j.quageo.2015.02.015.

Cundy, A.B., Croudace, I.W., Thomson, J., Lewis, J.T., 1997. Reliability of salt marshes as "Geochemical Recorders" of pollution input: a case study from contrasting estuaries in southern England. Environ. Sci. Technol. 31 (4), 1093–1101.

de Vet, P.L.M., van Prooijen, B.C., Colosimo, I., Steiner, N., Ysebaert, T., Herman, P.M.J., Wang, Z.B., 2020. Variations in storm-induced bed level dynamics across intertidal flats. Sci. Rep. 10, 12877. https://doi.org/10.1038/s41598-020-69444-7.

Environment Agency, 2011. The Extent of Saltmarsh in England And Wales: 2006–2009. Environment Agency, Bristol.

Fagherazzi, S., Mariotti, G., Leonardi, N., Canestrelli, A., Nardin, W., Kearney, W.S., 2020. Salt marsh dynamics in a period of accelerated sea level rise. J.Geophys.Res.Earth Surf. 125 (8), e2019JF005200.

FitzGerald, D.M., Fenster, M.S., Argow, B.A., Buynevich, I.V., 2008. Coastal impacts due to sea-level rise. Annu. Rev. Earth Planet. Sci. 36, 601–647. https://doi.org/10.1146/annurev.earth.35.031306.140139.

Galbraith, R.F., Roberts, R.G., Laslett, G.M., Yoshida, H., Olley, J.M., 1999. Optical dating of single and multiple grains of quartz from Jinmium rock shelter, northern Australia: part I,experimental design and statistical models. Archaeometry 41 (2), 339–364. https://doi.org/10.1111/j.1475-4754.1999.tb00987.x.

Ganju, N.K., Defne, Z., Kirwan, M.L., Fagherazzi, S., D'Alpaos, A., Carniello, L., 2017. Spatially integrative metrics reveal hidden vulnerability of microtidal salt marshes. Nat. Commun. 8. https://doi.org/10.1038/ncomms14156.

Godfrey-Smith, D.I., Huntley, D.J., Chen, W.-H., 1988. Optical dating studies of quartz and feldspar sediment extracts. Quat. Sci. Rev. 7, 373–380.

Grant, J., Turner, S.J., Legendre, P., Hume, T.M., Bell, R.G., 1997. Patterns of sediment reworking and transport over small spatial scales on an intertidal sandflat, Manukau Harbour, New Zealand. J. Exp. Mar. Biol. Ecol. 216, 33–50 PII S0022-0981(97)00089-0.

Gray, H.J., Tucker, G.E., Mahan, S.A., McGuire, C., Rhodes, E.J., 2017. On extracting sediment transport information from measurements of luminescence in river sediment. J.Geophys. Res.Earth Surf. 122, 654–677. https://doi.org/10.1002/2016JF003858.

Gray, H.J., Tucker, G.E., Mahan, S.A., 2018. Application of a luminescence-based sediment transport model. Geophys. Res. Lett. 45, 6071–6080. https://doi.org/10.1029/2018GL078210.

Gray, H.J., Jain, M., Sawakuchi, A.O., Mahan, S.A., Tucker, G.E., 2019. Luminescence as a sediment tracer and provenance tool. Rev. Geophys. 57. https://doi.org/10.1029/2019RG000646.

Haddadchi, A., Olley, J., Pietsch, T., 2016. Using LM-OSL of quartz to distinguish sediments derived from surface-soil and channel erosion. Hydrol. Process. 30 (4), 637–647. https://doi.org/10.1002/hyp.10646.

Hammer, O., 2019. PAST, Paleontological Statistics Version 3.25, Reference manual. Natural History Museum, University of Oslo.

Kirwan, M.L., Guntenspergen, G.R., D'Alpaos, A., Morris, J.T., Mudd, S.M., Temmerman, S., 2010. Limits on the adaptability of coastal marshes to rising sea level. Geophys. Res. Lett. 37. https://doi.org/10.1029/2010gl045489.

Leonardi, N., Carnacina, I., Donatelli, C., Ganju, N.K., Plater, A.J., Schuerch, M., Temmerman, S., 2018. Dynamic interactions between coastal storms and salt marshes: a review. Geomorphology 301, 92–107. https://doi.org/10.1016/j.geomorph.2017.11.001.

Li, B., Li, S.-H., 2011. Luminescence dating of K-feldspar from sediments: a protocol without anomalous fading correction. Quat. Geochronol. 6, 468e479. https://doi.org/10.1016/j.quageo.2011.05.001.

Lyons, M.G., 1997. The dynamics of suspended sediment transport in the Ribble estuary. Water AirSoil Pollut. 99 (1–4), 141–148. https://doi.org/10.1023/a:1018388517409.

Mariotti, G., Fagherazzi, S., 2010. A numerical model for the coupled long-term evolution of salt marshes and tidal flats. J. Geophys. Res. Earth Surf. 115 (F1). https://doi.org/10.1029/2009JF001326.

McCloskey, T.A., Liu, K., 2012. A 7000 year record of paleohurricane activity from a coastal wetland in Belize. The Holocene 23 (2), 278–291. https://doi.org/10.1177/0959683612460782.

Möller, I., Spencer, T., French, J.R., Leggett, D.J., Dixon, M., 1999. Wave transformation over salt marshes: a field and numerical modelling study from north Norfolk,England. Estuar. Coast. Shelf Sci. 49 (3), 411–426. https://doi.org/10.1006/ecss.1999.0509.

Mudd, S.M., D'Alpaos, A., Morris, J.T., 2010. How does vegetation affect sedimentation on tidal marshes? Investigating particle capture and hydrodynamic controls on biologically mediated sedimentation. J.Geophys.Res.Earth Surf. 115. https://doi.org/10.1029/2009jf001566.

Murray, A.S., Arnold, L.J., Buylaert, J.-P., Guerin, G., Qin, J., Singhvi, A.K., Smedley, R.K., Thomsen, K.J., 2021. Optically stimulated luminescence dating using quartz. Nat.Rev. Methods Primers 1, 72. https://doi.org/10.1038/s43586-021-00068-5.

Neumeier, U., Ciavola, P., 2004. Flow resistance and associated sedimentary processes in a Spartina maritima salt-marsh. J. Coast. Res. 20 (2), 435–447. https://doi.org/10.2112/1551-5036(2004)020[0435:fraasp]2.0.co;2.

Pannozzo, N., Leonardi, N., Carnacina, I., Smedley, R., 2021a. Dataset of results from numerical simulations of increased storm intensity in an estuarine salt marsh system. DataBr. 38 (6), 107336. https://doi.org/10.1016/j.dib.2021.107336.

Pannozzo, N., Leonardi, N., Carnacina, I., Smedley, R., 2021b. Salt marsh resilience to sea-level rise and increased storm intensity. Geomorphology 389 (4), 107825. https://doi.org/10.1016/j.geomorph.2021.107825.

Pannozzo, N., Smedley, R., Chiverrell, R., Carnacina, I., Leonardi, N., 2022. An integration of numerical modelling and paleoenvironmental analysis reveals the effects of embankment construction on long-term salt marsh accretion. J.Geophys.Res.Earth Surf. 127, e2021JF006524.

Pethick, J., 1981. Long-term accretion rates on tidal salt marshes. J. Sediment. Res. 51 (2), 571–577. https://doi.org/10.1306/212F7CDE-2B24-11D7-8648000102C1865D.

Plater, A.J., Huddart, D., Innes, J.B., Pye, K., Smith, A.J., Tooley, M.J., 1993. Coastal and sea-level changes. In: Atkinson, D., Houston, J. (Eds.), The Sand Dunes of the Sefton Coast. NMGM, Liverpool, pp. 23–34.

Plater, A.J., Ridgway, J., Rayner, B., Shennan, I., Horton, B.P., Haworth, E.Y., Wright, M.R., Rutherford, M.M., Wintle, A.G., 2000. Sediment provenance and flux in the Tees Estuary: the record from the Late Devensian to the present. Geol. Soc. 166, 171–195. https://doi.org/10.1144/GSL.SP.2000.166.01.10.

Plater, A.J., Stupples, P., Roberts, H.M., 2007. The depositional history of the Dungeness Foreland. In: Long, A.J., Walker, M.P., Plater, A.J. (Eds.), The Late Holocene Evolution of the Romney Marsh/Dungeness Foreland Depositional Complex, UK. Oxbo Books, Oxford.

PSMSL, 2019. Permanent Service for Mean Sea Level. https://www.psmsl.org/.

Pye, K., Neal, A., 1994. Coastal dune erosion at Formby Point, north Merseyside, England - causes and mechanisms. Mar. Geol. 119 (1–2), 39–56. https://doi.org/10.1016/0025-3227(94)90139-2.

Rahman, R., Plater, A.J., 2014. Particle-size evidence of estuary evolution: a rapid and diagnostic tool for determining the nature of recent saltmarsh accretion. Geomorphology 213, 139–152. https://doi.org/10.1016/j.geomorph.2014.01.004.

Reed, D.J., 1990. The impact of sea-level rise on coastal salt marshes. Prog. Phys. Geogr. 14 (4), 465–481. https://doi.org/10.1177/030913339001400403.

Reimann, T., Notenboom, P.D., De Schipper, M.A., Wallinga, J., 2015. Testing for sufficient signal resetting during sediment transport using a polymineral multiple-signal luminescence approach. Quat. Geochronol. 25, 26–36.

Roberts, H.M., Plater, A.J., 2005. Optically Stimulated Luminescence (OSL) Dating of Sands Underlying the Gravel Beach Ridges of Dungeness And Camber, Southeast England, UK. Centre for Archaeology Report, p. 27.

Sawakuchi, A.O., Blair, M.W., DeWitt, R., Faleiros, F.M., Hyppolito, T., Guedes, C.C.F., 2011. Thermal history versus sedimentary history: OSL sensitivity of quartz grains extracted from rocks and sediments. Quat. Geochronol. 6 (2), 261–272.

Sawakuchi, A.O., Guedes, C.C.F., DeWitt, R., Giannini, P.C.F., Blair, M.W., Nascimento, D.R., Faleiros, F.M., 2012. Quartz OSL sensitivity as a proxy for storm activity on the southern Brazilian coast during the Late Holocene. Quat. Geochronol. 13, 92–102.

Sawakuchi, A.O., Jain, M., Mineli, T.D., Nogueira, L., Bertassoli, D.J., Häggi, C., et al., 2018. Luminescence of quartz and feldspar fingerprintsprovenance and correlates with the source area denudation in the Amazon River basin. Earth Planet. Sci. Lett. 492, 152–162. https://doi.org/10.1016/j.epsl.2018.04.006.

Schuerch, M., Vafeidis, A., Slawig, T., Temmerman, S., 2013. Modeling the influence of changing storm patterns on the ability of a salt marsh to keep pace with sea level rise. J.Geophys.Res.Earth Surf. 118 (1), 84–96. https://doi.org/10.1029/2012jf002471.

Scourse, J.D., Chiverrell, R.C., Smedley, R.K., Small, D., Burke, M.J., Saher, M., Van Landeghem, K.J.J., Duller, G.A.T., Cofaigh, C.Ó., Bateman, M.D., Benetti, S., Bradley, S., Callard, L., Evans, D.J.A., Fabel, D., Jenkins, G.T.H., McCarron, S., Medialdea, A., Moreton, S., Ou, X., Praeg, D., Roberts, D.H., Roberts, H.M., Clark, C.D., 2021. Maximum extent and readvance dynamics of the Irish Sea Ice Stream and Irish Sea Glacier since the Last Glacial Maximum. J. Quat. Sci. 36 (5), 780–804. https://doi.org/10.1002/jqs.3313.

Shennan, I., Bradley, S.L., Edwards, R., 2018. Relative sea-level changes and crustal movements in Britain and Ireland since the Last Glacial Maximum. Quat. Sci. Rev. 188, 143–159. https://doi.org/10.1016/j.quascirev.2018.03.031.

Smedley, R.K., 2018. Telling the time with dust, sand and rocks. Elements 14, 9–14.

Smedley, R.K., Duller, G.A.T., Roberts, H.M., 2015. Bleaching of the post-IR IRSL signal from individual grains of K-feldspar: implications for single-grain dating. Radiat. Meas. 79, 33e42. https://doi.org/10.1016/j.radmeas.2015.06.003.

Temmerman, S., Meire, P., Bouma, T.J., Herman, P.M.J., Ysebaert, T., De Vriend, H.J., 2013. Ecosystem-based coastal defence in the face of global change. Nature 504 (7478), 79–83. https://doi.org/10.1038/nature12859.

Temmerman, S., Horstman, E.M., Krauss, K.W., Mullarney, J.C., Pelckmans, I., Schoutens, K., 2022. Marshes and mangroves as nature-based coastal storm buffers. Annu. Rev. Mar. Sci. 15 (9), 1–24. https://doi.org/10.1146/annurev-marine-040422-092951.

Thomsen, K.J., Murray, A., Jain, M., Bøtter-Jensen, L., 2008. Laboratory fading rates of various luminescence signals from feldspar-rich sediment extracts. Radiat. Meas. 43, 1474–1486. https://doi.org/10.1016/j.radmeas.2008.06.002.

Tooley, M., 1974. Sea level changes during the last 9000 years in northwest England. J. Geogr. 140, 18–42.

Tovey, E.L., Pontee, N.I., Harvey, R., 2009. Managed realignment at Hesketh Out Marsh West. Proc. Inst. Civ. Eng. Eng. Sustain. 162 (4), 223–228. https://doi.org/10.1680/ensu.2009.162.4.223.

UK MET Office, 2021. Weather and climate. Warnings and advice. UK Strom Centre. https://www.metoffice.gov.uk/weather/warnings-and-advice/uk-storm-centre/index.

UKHO, 2001. Admiralty Tide Tables. United Kingdom and Ireland (Including European Channel Ports). UK Hydrographic Office, Taunton. https://www.admiralty.co.uk/publications/publications-and-reference-guides/admiralty-tide-tables.

van der Wal, D., Pye, K., Neal, A., 2002. Long-term morphological change in the Ribble Estuary, northwest England. Mar. Geol. 189 (3–4), 249–266. https://doi.org/10.1016/s0025-3227(02)00476-0.

Van Landeghem, K.J.J., Chiverrell, R.C., 2020. Bed erosion during fast ice streaming regulated the retreat dynamics of the Irish Sea Ice Stream. Quat. Sci. Rev. 245. https://doi.org/10.1016/j.quascirev.2020.106526.

Van Landeghem, K.J.J., Baas, J., Mitchell, N., Wilcockson, D., Wheeler, A., 2012. Sediment wave migration in the Irish Sea, NW Europe: a reappraisal of the validity of geometry-based predictive modelling and assumptions. Mar. Geol. 295–298, 95–112. https://doi.org/10.1016/j.margeo.2011.12.004.

van Proosdij, D., Davidson-Arnott, R.G.D., Ollerhead, J., 2006. Controls on spatial patterns of sediment deposition across a macro-tidal salt marsh surface over single tidal cycles. Estuar. Coast. Shelf Sci. 69, 64–86. https://doi.org/10.1016/j.ecss.2006.04.022.

Wallinga, J., 2002a. Detection of OSL age overestimation using single-aliquot techniques. Geochronometria 21, 17–20.

Wallinga, J., 2002b. Optically stimulated luminescence dating of fluvial deposits: a review. Boreas 31, 303–322 ISSN 0300-9483.

Wallinga, J., Murray, A., Wintle, A., 2000. The single-aliquot regenerative-dose (SAR) protocol applied to coarse-grain feldspar. Radiat. Meas. 32 (5–6), 529–533. https://doi.org/10.1016/S1350-4487(00)00091-3.

Walters, D.C., Kirwan, M.L., 2016. Optimal hurricane overwash thickness for maximizing marsh resilience to sea level rise. Ecol.Evol. 6 (9), 2948–2956. https://doi.org/10.1002/ece3.2024.

Wesselman, D., de Winter, R., Engelstad, A., McCall, R., van Dongeren, A., Hoekstra, P., Oost, A., van der Vegt, M., 2017. The effect of tides and storms on the sediment transport across a Dutch barrier island. Earth Surf. Process. Landf. 43 (3), 579–592. https://doi.org/10.1002/esp.4235.

Woodworth, P.L., Tsimplis, M.N., Flather, R.A., Shennan, I., 1999. A review of the trends observed in British Isles mean sea level data measured by tide gauges. Geophys. J. Int. 136, 651–670. https://doi.org/10.1046/j.1365-246x.1999.00751.x.

Wright, J.E., Hull, J.H., McQuillin, R., Arnold, S.E., 1971. Irish Sea Investigations 1969-71. NERC Institute of Geological Sciences Report 71/19.

Yang, S.L., Shi, B.W., Bouma, T.J., Ysebaert, T., Luo, X.X., 2012. Wave attenuation at a salt marsh margin: a case study of an exposed coast on the Yangtze Estuary. Estuar. Coasts 35, 169–182. https://doi.org/10.1007/s12237-011-9424-4.

Yang, S.L., Luo, X., Temmerman, S., Kirwan, M., Bouma, T., Xu, K., Zhang, S., Fan, J., Shi, B., Yang, H., Wang, Y.P., Shi, X., Gaoet, S., 2020. Role of delta-front erosion in sustaining salt marshes under sea-level rise and fluvial sediment decline. Limnol. Oceanogr. 65 (9), 1990–2009. https://doi.org/10.1002/lno.11432.

Zhang, X., Leonardi, N., Donatelli, C., Fagherazzi, S., 2019. Fate of cohesive sediments in a marsh-dominated estuary. Adv. Water Resour. 125, 32–40. https://doi.org/10.1016/j.advwatres.2019.01.003.